sensors

MDPI

Letter

Adsorption Properties of Pd_3-Modified Double-Vacancy Defect Graphene toward SF_6 Decomposition Products

Jie Li, Lei Pang *, Fuwei Cai, Xieyu Yuan and Fanyu Kong

School of Electrical Engineering, Xi'an Jiaotong University, Xi'an 710049, China; jl1562074348@stu.xjtu.edu.cn (J.L.); za41255@stu.xjtu.edu.cn (F.C.); yxy201115010@163.com (X.Y.); kfy3119104175@stu.xjtu.edu.cn (F.K.)

* Correspondence: panglei_2013@mail.xjtu.edu.cn; Tel.: +86-186-2938-9017

Received: 30 June 2020; Accepted: 22 July 2020; Published: 28 July 2020

Abstract: In this study, we investigate Pd_3-cluster-modified 555–777 graphene (Pd_3-graphene) as a novel resistor-type gas sensor to detect SF_6 decomposition products based on density functional theory calculations. We obtained and minutely analyzed the relevant parameters of each most stable adsorption configuration to explore the microscopic mechanism during gas adsorption. Theoretical results reveal that Pd_3-graphene shows great adsorption capacity and sensitivity toward those decompositions. High adsorption energies and abundant charge transfer amounts could guarantee a stable adsorption structure of decomposition gases on Pd_3-graphene surface. The complex change of density of states verifies a strong chemical reaction between the gases and the surface. Moreover, the conductivity of Pd_3-graphene would improve due to the decrease of energy gap, and the sensitivity was calculated as $SOF_2 > H_2S > SO_2 > SO_2F_2$. This work provides an effective method to evaluate the operation status of SF_6 gas-insulated equipment.

Keywords: Pd_3-graphene; SF_6 decomposition products; DFT; adsorption

1. Introduction

Owing to its outstanding insulation and arc-extinguishing properties, SF_6 has been widely applied in gas-insulated switchgear (GIS) [1,2]. However, in the long-term operation of GIS, several inevitable insulation defects may cause partial discharge and partial overheat, which will lead to the initial decomposition of SF_6 [3,4]. Simultaneously, SF_6 will ultimately decompose to several characteristic products with the reaction of trace O_2 and H_2O in SF_6-insulated equipment: H_2S, SO_2, SOF_2 and SO_2F_2 gas [5–7]. These decomposition products can corrode the metal parts inside the equipment, accelerate the aging of the insulation medium—and even result in the sudden failure of GIS [8,9]. Therefore, discovering SF_6 decomposition products and dealing with insulation defects in a timely manner have great importance. To date, several methods such as gas chromatography, mass spectrometry and Fourier transform infrared spectroscopy, are suggested to detect SF_6 products [10,11]. However, these methods are either inaccurate or complicated, so none of them are used in detecting SF_6 decomposition products.

In recent years, the gas sensor method has been used in various fields due to its advantages such as high sensitivity, rapid response and small size. Graphene is a 2D material with a unique 2D monoatomic layer structure and an electronic energy band structure. Its excellent characteristics—including high electron mobility, high thermal conductivity, brilliant mechanical properties and large specific surface area—make it a promising gas sensor material [12–17]. However, in actual production, several intrinsic defects in graphene may be observed, such as single defects, double-vacancy defects and Stone–Wales defects [18]. Lattice defects may cause local charge traps on the graphene surface, which has a

substantial effect on improving the electronic structure and the adsorption capacity of graphene. Liu et al. anchored Sc, Zn, Mo, Ru, Rh, Pd and Ag atoms on defective graphene for N_2 reduction reaction and found that a single Mo embedded on nitrogen-doped 555–777 graphene shows eminent catalytic performance [19]. Arokiyanathan et al. calculated the adsorption properties of small Li clusters on graphene with Stone–Wales defect. The results showed that Li clusters have a strong interaction with the defect region [20]. Ma et al. reported hydrogen adsorption on Co-4-doped defective graphene and discovered that point defects in graphene can effectively improve the hydrogen storage capacity of Co-4 [21]. Despite much research on defective graphene [22–25], few relevant research on SF_6 decomposition product detection have been reported.

555–777 graphene is a double-vacancy defect graphene sheet [18]. The absence of two carbon atoms does not destroy the original SP^2 hybrid orbital network but forms a stable topological hole. Thus, 555–777 graphene has a more stable electronic structure compared with other defective structures. Previous studies showed that doping transition metal elements on graphene surface can improve its electrical conductivity and enhance its capacity to adsorb gas molecules [26–30]. Liu et al. calculated the adsorption of SF_6 decompositions on Pd (111) surface and found that Pd (111) would have great adsorption capacity on absorbing those products. Thus, doping Pd element on 555–777 graphene may be a potential method to improve its adsorption properties [30]. In this study, Pd_3-doped 555–777 graphene (Pd_3-graphene) is carried out to detect SF_6 decomposition products (H_2S, SO_2, SOF_2 and SO_2 F_2). Different adsorption structures of each gas are obtained to find the most stable adsorption structure. Furthermore, adsorption energy, charge transfer, density of states (DOS) and deformation charge density (DCD) of Pd_3-graphene surface before and after gas adsorption are calculated to reveal the gas response mechanism. Overall, our work aims to provide some theoretical basis for developing a novel graphene sensor.

2. Computational Details and Models

In this work, all calculations are carried out using $Dmol^3$ package based on density functional theory (DFT) [31]. Generalized gradient approximation and Perdew–Burke–Ernzerhof function are utilized to deal with the electron exchange-correlation energy and interaction effect of electrons [32,33]. DFT semi-core pseudopots are set to recoup the relativistic effect of Pd atoms. The Brillouin zone is sampled with $6 \times 6 \times 1$ k-points in the Monkhorst–Pack grid [34]. Double numeric plus polarization basis sets are used to obtain a higher calculation precision of hydrogen bond [35]. The smearing is set as 0.001 Ha to ensure the accuracy of the DFT calculation. The SCF tolerance is 1×10^{-6} Ha and spin polarization is considered due to the magnetic properties of Pd atoms. Additionally, total energy of convergence tolerance, maximum force and maximum displacement are set as 1×10^{-5} Ha, 2×10^{-3} Ha/Å and 5×10^{-3} Å, respectively.

Intrinsic 555–777 graphene surface consists of a 6×6 supercell, and the lattice parameter is 14.760 Å × 14.760 Å. The vacuum area is set as 20 Å to avoid the interaction of neighboring slabs. The Pd_3 cluster is a triangular structure composed of three Pd atoms. Through DFT calculations, various parameters of stable adsorption structures can be acquired, including adsorption energy (E_{ad}), charge transfer amount (Q_T), adsorption distance (D) and energy gap (E_g). The definition of these parameters are the same as the previous study [36].

3. Results and Discussions

3.1. Geometric Optimization

We apply geometric optimization to minimize their energy and obtain the most stable status of H_2S, SO_2, SOF_2, SO_2 F_2 and Pd_3-graphene. The optimized structures are shown in Figure 1 (adapted from [36]). Figure 1a shows the stable structure of intrinsic 555–777 graphene with three pentagons and heptagons at the center of the graphene sheet. Considering that the charge trap in the center of the hole has a strong binding ability to electrons and the special D electronic structure of Pd metal,

we dope the Pd_3 cluster at the defect center of graphene to form a stable anchored structure. Figure 1b shows that the Pd_3 cluster is parallel to the graphene surface, indicating that the force of the crystal plane on the three Pd atoms is almost equal. Bond lengths between the Pd atoms are 2.714, 2.714 and 2.812 Å. Millikan charge analysis shows that 0.16 electrons transfer from the Pd_3 cluster to the graphene sheet after geometric optimization, showing an evident orbital hybridization between C and Pd atoms. The electronic structure of the graphene surface will be greatly changed, which may substantially improve gas adsorption capacity.

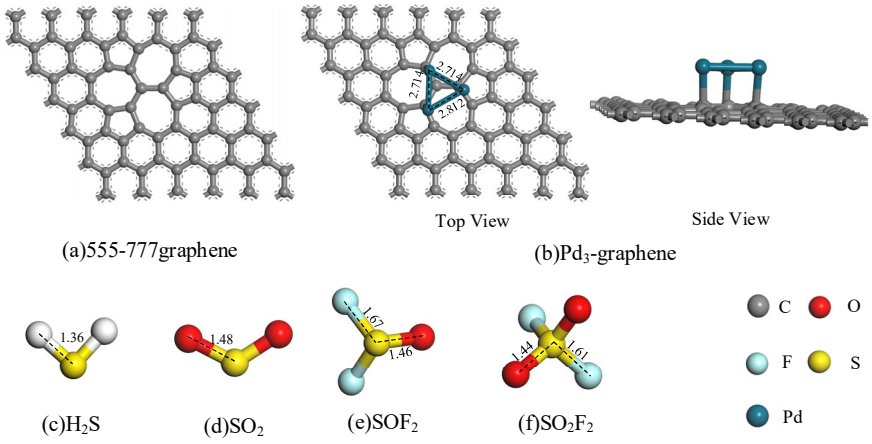

Figure 1. Optimized structures of intrinsic 555–777 graphene, Pd_3-graphene and gas molecules (distance in Å). © 2020 IEEE.

3.2. Adsorption Systems

3.2.1. H_2S Adsorption on Pd_3-Graphene

The H_2S molecule is placed in different distances and angles to approach the Pd_3-graphene surface and obtain the most stable adsorption structure of H_2S gas. Considering the symmetry of H_2S molecule, its two typical stable adsorption structures are acquired through H and S atoms approaching the Pd_3-graphene surface, as shown in Figure 2. E_{ad}, Q_T and D are listed in Table 1.

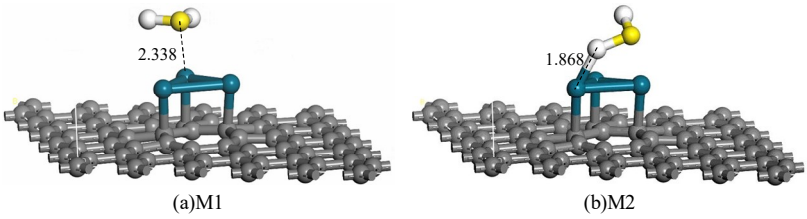

Figure 2. Adsorption structures of H_2S on Pd_3-graphene surface (distance in Å).

Table 1. Structural parameters of H_2S adsorption systems on Pd_3-graphene surface. Position represents the approaching way, for instance, S–Pd means the H_2S molecule approaches the Pd atom by the S atom.

System	Position	E_{ad} (eV)	Q_T (e)	D (Å)
M1	S–Pd	−1.211	0.286	2.338
M2	H–Pd	−1.185	0.279	1.868

Figure 2a shows the adsorption configuration of system M1. The H_2S molecule approaches the surface by the S atom and forms a stable interaction between the S and Pd atoms. The D of M1 is 2.338 Å, revealing that the reaction is relatively strong. When the adsorption energy is greater than 0.6 eV, the adsorption is generally considered chemical. The corresponding E_{ad} of M1 is −1.211 eV; hence,

the adsorption is chemical, and the process is spontaneous. The positive value of Q_T of M1 (0.286) demonstrates that 0.286 electrons transfer from the H_2S molecule to the Pd_3-graphene.

In Figure 2b, the H_2S molecule approaches the Pd_3-graphene by H atom, forming a new ionic bond with the Pd atom. The length of the H–Pd bond is 1.868 Å, indicating a strong chemical interaction between H and Pd atoms. Similar to system M1, 0.279 electrons transfer from the H_2S molecule to the sheet during optimization. The E_{ad} of system M2 (−1.185 eV) is smaller than that of M1 (−1.211 eV), which means that system M1 releases more energy than M2 after H_2S adsorption. Above all, according to the greater E_{ad} and Q_T of configuration M1, M1 is the most stable adsorption structure of H_2S on Pd_3-graphene surface.

DOS and partial density of states (PDOS) of the most stable adsorption structure (M1) are calculated to analyze the mechanism of H_2S adsorption further, as shown in Figure 3. In Figure 3a, the black and red lines represent the DOS before and after H_2S adsorption, respectively. Several distinct changes are observed in DOS after H_2S adsorption, which mainly reflect in the increase of DOS from −8 eV to −4 eV. The DOS at the Fermi level rises slightly, revealing that electrons can more easily transfer from the valence band to the conduction band, which may have a substantial effect on improving its conductivity. The PDOS in Figure 3b shows that the increased area of DOS from −8 eV to −4 eV mainly consists of the 3p orbit of S atom. The large overlapped area from −7 eV to −3 eV between the 4d orbit of Pd atom and the 3p orbit of S atom manifests that the chemical reaction between these atoms is strong, which is consistent with the above analysis.

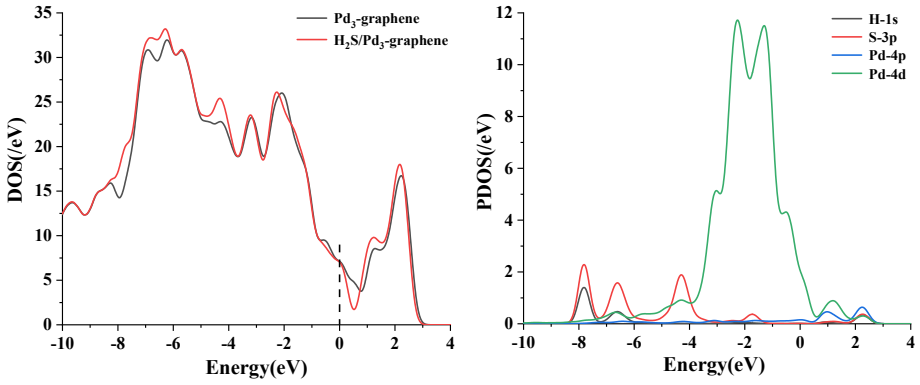

(a)DOS of M1 structure (b)PDOS of M1 structure

Figure 3. Density of states (DOS) and partial density of states (PDOS) of system M1. Dashed line represents the Fermi level.

3.2.2. SO_2 Adsorption on Pd_3-Graphene

For the adsorption of SO_2 on Pd_3-graphene surface, various initial positions of SO_2 molecule are set to investigate the most stable adsorption system. After geometric optimization, two typical stable adsorption configurations are obtained. Figure 4 shows the adsorption structures through S and O atoms approaching the sheet. Figure 4a shows that the SO_2 molecule forms a stable adsorption structure by building a chemical bond between S and Pd atoms. The length of the S–Pd bond is 2.192 Å, declaring a strong interaction between them. The two O atoms are far from the sheet; thus, no direct interaction may exist between them and the crystal plane. In Figure 4b the SO_2 molecule approaches the Pd_3 cluster by O atoms, forming two chemical bonds with the Pd atoms. The length of both O–Pd bonds is 2.131 Å, which is shorter than that of the S–Pd bond in system M3. Thus, the chemical reaction in system M4 may be stronger than that in M3.

Table 2 presents the related parameters of configuration M3 and M4. Both their E_{ad} are negative, manifesting that the adsorption is exothermic and proceeds spontaneously. By contrast, the E_{ad} of system M4 is greater than that of system M3, implying that the SO_2 molecule absorbed on the Pd_3-graphene surface through two O atoms is the most stable structure. Given the strong reaction

between O and Pd atoms in system M4, 0.283 electrons transfer from the sheet to SO_2 molecule. For system M3, the small Q_T means that the ionic S–Pd bond is relatively easy to break.

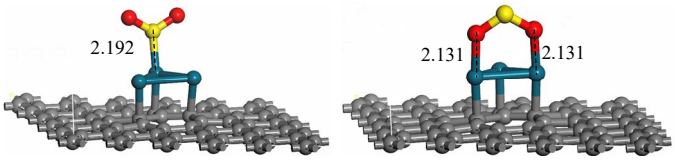

(a)M3 (b)M4

Figure 4. Adsorption structures of SO_2 on Pd_3-graphene surface (distance in Å).

Table 2. Structural parameters of SO_2 adsorption systems on Pd_3-graphene surface. Position represents the approaching way, for instance, S–Pd means the SO_2 molecule approaches the Pd atom by the S atom.

System	Position	E_{ad} (eV)	Q_T (e)	D (Å)
M3	S–Pd	−1.534	−0.023	2.192
M4	O–Pd	−1.591	−0.283	2.131

The DOS and PDOS of M4 are intensively calculated to analyze the adsorption mechanism because M4 is the most stable adsorption configuration of SO_2 on Pd_3-graphene. Figure 5a presents that the DOS of M4 exhibits three new peaks after SO_2 adsorption at around −8, −6 and −4 eV. PDOS shows that the new peaks mainly result from the 2p orbit of O atom and the 3p orbit of S atom. The small increase of DOS at fermi level demonstrates an increase of the conductivity of Pd_3-graphene. In addition, a large overlapped area between the 2p orbit of O atom and the 4d orbit of Pd atom ranges from −5 eV to −3 eV, reflecting a complex hybridization of those orbits. Therefore, the chemical reaction between O atoms and Pd atom is strong enough to form a stable adsorption configuration.

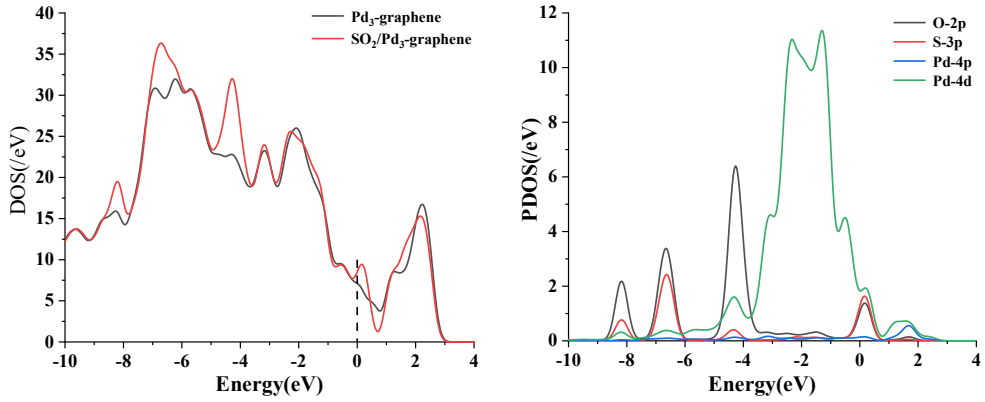

(a)DOS of M4 structure (b)PDOS of M4 structure

Figure 5. Density of states (DOS) and partial density of states (PDOS) of system M4. Dashed line represents the Fermi level.

3.2.3. SOF_2 Adsorption on Pd_3-Graphene

Subsequently, we place the SOF_2 molecule in different directions and distances approaching the sheet to explore the most stable adsorption structure. Figure 6 shows three typical adsorption configurations, in which the SOF_2 molecule is absorbed on Pd_3-graphene surface by S, F and O atoms. Related parameters are listed in Table 3.

Figure 6a shows that the SOF_2 molecule approaches the surface by the S atom and forms a stable adsorption structure ultimately. The S atom is trapped by the Pd atom and builds a new chemical bond with a bond length of 2.170 Å. The E_{ad} of system M5 listed in Table 3 is −1.230 eV, which indicates that the adsorption is chemical, and the structure is stable enough. During adsorption, only 0.038 electrons

transfer from SOF_2 molecule to the sheet, so their electronic structure may change slightly. For system M6 shown in Figure 6b, SOF_2 molecule absorbs on the Pd_3-graphene surface by forming an ionic bond length of 2.124 Å between F and Pd atoms. The E_{ad} of M6 (−0.284 eV) is smaller than that of M5 (−1.230 eV), revealing that M5 is more stable than M6. In system M7, the SOF_2 molecule absorbs directly above the hollow position of Pd_3 cluster. The length of the O–Pd bond is 2.299 Å, which is longer than that of M5 and M6. However, the specific E_{ad} of M7 (−1.282 feV) is greater than that of M5 (−1.230 eV), implying that system M7 is more stable. Opposite to system M5, 0.132 electrons transfer from the sheet to SOF_2 molecule after absorbing on Pd_3-graphene. Hence, the SOF_2 molecule tends to be absorbed on the Pd_3-graphene surface in the form of M7, establishing an adsorption system with the lowest energy.

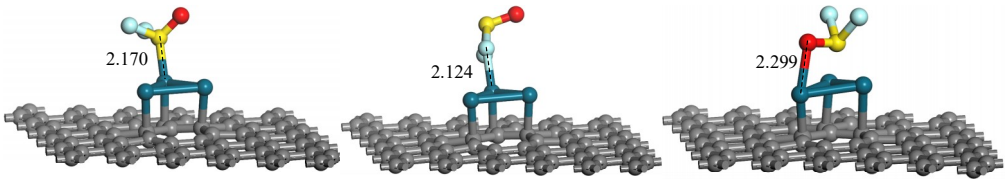

(a)M5 (b)M6 (c)M7

Figure 6. Adsorption structures of SOF_2 on Pd_3-graphene surface (distance in Å).

Table 3. Structural parameters of SOF_2 adsorption systems on Pd_3-graphene surface. Position represents the approaching way, for instance, S–Pd means the SOF_2 molecule approaches the Pd atom by the S atom.

System	Position	E_{ad} (eV)	Q_T (e)	D (Å)
M5	S–Pd	−1.230	0.038	2.170
M6	F–Pd	−0.284	−0.255	2.124
M7	O–Pd	−1.282	−0.132	2.299

Figure 7 shows the DOS and PDOS of the most stable adsorption structure of SOF_2 on the Pd_3-graphene surface. The DOS of M7 structure increases distinctly in the range from −9 eV to −7.5 eV and −6 eV to −3 eV after SOF_2 adsorption. These changes are mainly caused by the 2p orbit of O atom and the 2p orbit of F atom. A slight increase of DOS near the fermi level is observed, signifying that SOF_2 adsorption can improve the conductivity of Pd_3-graphene. The PDOS displaces the hybridization of individual atoms during adsorption. The 2p orbit of O atom, the 2p of F atom and the 4d orbit of Pd atom overlap from −6 eV to −1 eV, suggesting that the chemical reaction between them is considered strong, and the electronic structure of the SOF_2 molecule is active.

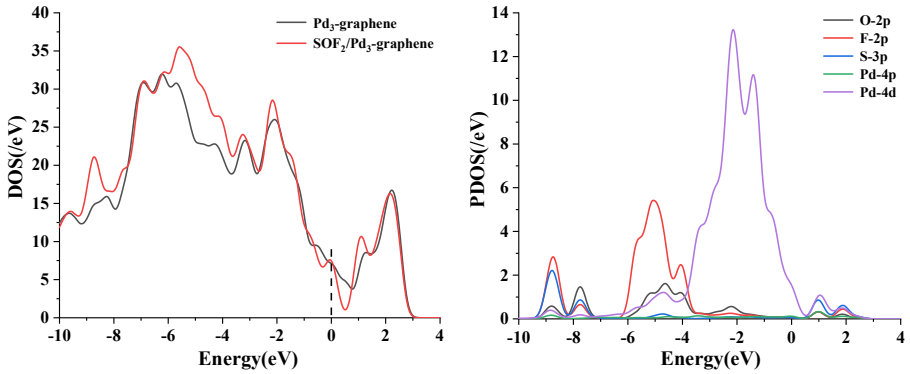

(a)DOS of M7 structure (b)PDOS of M7 structure

Figure 7. Density of states (DOS) and partial density of states (PDOS) of system M7. Dashed line represents the Fermi level.

3.2.4. SO_2F_2 Adsorption on Pd_3-Graphene

Eventually, the SO_2F_2 molecule approaches the Pd_3-graphene surface in various directions and distances to find the most stable adsorption structure. After adsorption structure optimization, two typical adsorption systems are obtained, as shown in Figure 8. Correlative parameters of adsorption systems are listed in Table 4.

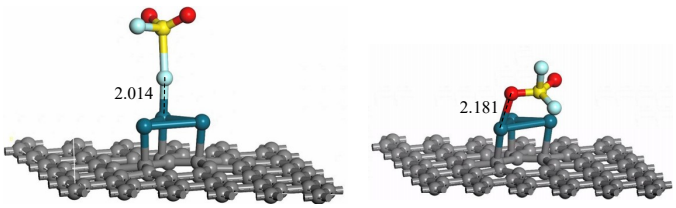

(a)M8 (b)M9

Figure 8. Adsorption structures of SO_2F_2 on Pd_3-graphene surface (distance in Å).

Table 4. Structural parameters of SO_2F_2 adsorption systems on Pd_3-graphene surface. Position represents the approaching way, for instance, F–Pd means the SO_2F_2 molecule approaches the Pd atom by F atom.

System	Position	E_{ad} (eV)	Q_T (e)	D (Å)
M8	F–Pd	−0.920	−0.705	2.014
M9	O–Pd	−0.804	−0.294	2.181

Figure 8a presents the adsorption configuration of SO_2F_2 molecule approaching the Pd_3-graphene surface by F atom. The Pd atom builds a chemical connection with the F atom during the approaching process and forms an F–Pd bond with length of 2.014 Å ultimately. The S–F bond is stretched to 2.40 Å due to the radial force of the Pd atom. In system M9, the SO_2F_2 molecule approaches the sheet by O atom. Similarly, the O atom forms a chemical bond with the Pd atom, but the length of the O–Pd bond (2.181 Å) is longer than that of the F–Pd bond (2.014 Å), implying a stronger interaction in configuration M8. The E_{ad} of M8 (−0.920 eV) is greater than that of M9 (−0.804 eV), demonstrating that the M8 structure is more stable than the M9 structure. Additionally, 0.705 electrons transfer from the sheet to the SO_2F_2 molecule in M8, which is 2.4 times of M9, confirming a stronger oxidation of the F atom. Thus, configuration M8 is supposed to be the most stable adsorption structure of SO_2F_2 on the Pd_3-graphene surface.

Figure 9a shows that DOS increases substantially in the range of −7 to 0.5 eV. PDOS reveals that the 2p orbit of O atom and the 2p orbit of F atom mainly contribute the increased area, that is, the DOS near the fermi level rises slightly. Thus, the conductivity of Pd_3-graphene is expected to improve after SO_2F_2 adsorption. According to the PDOS, a large hybridization is observed between the 2p orbit of F atom and the 4d orbit of Pd atom from −5 eV to −1 eV, implying that these orbits are relatively active, while SO_2F_2 approaches the surface.

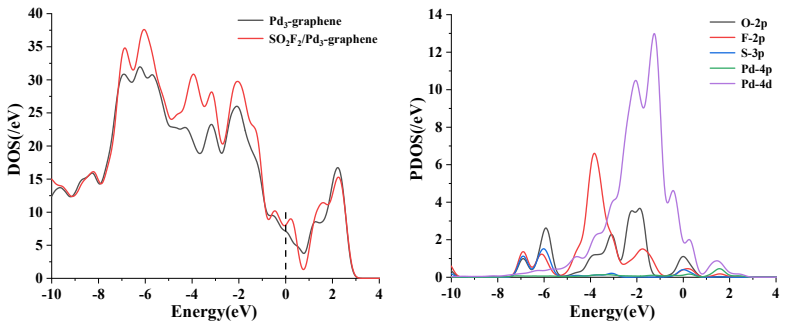

(a)DOS of M8 structure (b)PDOS of M8 structure

Figure 9. Density of states (DOS) and partial density of states (PDOS) of system M8. Dashed line represents the Fermi level.

3.2.5. SF_6 Adsorption on Pd_3-Graphene

In order to ensure that the Pd_3-graphene sensor can be utilized in GIS, we further calculated the adsorption of SF_6 gas on Pd_3-graphene surface to eliminate the interference of SF_6 gas. Same as other gases, SF_6 approaches the graphene surface at different angles and distances. After the geometric optimization, we obtained the most stable adsorption structure of SF_6 on Pd_3-graphene surface shown in Figure 10. As presented, SF_6 molecule approaches the Pd_3-graphene surface by F atom and forms a weak interaction with the Pd atom. The adsorption distance of SF_6 is 4.060 Å, which is longer than other gases. Moreover, the E_{ad} of SF_6 is calculated to be–0.124 eV, reflecting that the adsorption the adsorption system is not stable enough. During the adsorption, 0.162 electrons transfer from the Pd_3-graphene to SF_6 molecule. In conclusion, the Pd_3-graphene can be a potential sensor applied in the SF_6 gas-insulated equipment.

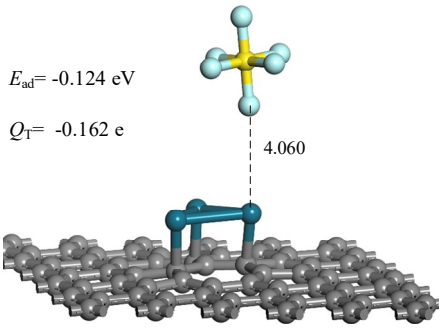

Figure 10. The most adsorption structure of SF_6 on Pd_3-graphene surface (distance in Å).

3.3. Electronic Properties

The deformation charge density of pure Pd_3-graphene and the four most stable adsorption systems is calculated to investigate the difference in electronic structure before and after modifying or gas adsorption. As presented in Figure 11, the red region means an increase of charge density after adsorption, whereas the blue region means a decrease. In Figure 11a, the charge density of Pd_3 cluster decreases, revealing that the defect of 555–777 graphene has a strong oxidation during the doping process. Although the absence of carbon atoms do not give rise to dangling bonds, the reconstruction of the graphene structure results in the change of bond lengths. Meanwhile, the defect would cause a rehybridization of the sigma and pi orbitals of carbon atoms, which would enhance the electron activity near the defect. When the transition metal approaches the defect, its special d electrons form a strong chemical interaction with the defect. Figure 11b shows that the charge density of the two Pd atoms decreases, while the S atom receives electrons from the Pd_3 cluster after adsorption. Therefore, the adsorption reaction is concentrated between the S atom and the Pd atom. In Figure 11c, electrons transfer from the Pd atoms to the O atom due to the strong electronegativity of the O atom, indicating that the two O–Pd bonds are stable enough to support the adsorption structure. The O atom also receives electrons from the S atom, such that the electronic structure inside the SO_2 gas changes prominently. As for SOF_2 gas, the charge density neighboring the O atom increases to a certain degree, and the charge density of the Pd atom decreases. In principle, the O atom performs as an electron acceptor during SOF_2 adsorption. In Figure 11e, the DCD of system M8 shows that the F atom receives electrons from the Pd atom and the nearby the S atom, verifying the fairly strong oxidability of the F atom. In conclusion, the Pd_3 cluster behaves as an electron donator during gas adsorption and leads to a violent chemical reaction in the vicinity, certifying that the Pd_3 dopant can substantially enhance the adsorption capacity of intrinsic 555–777 graphene.

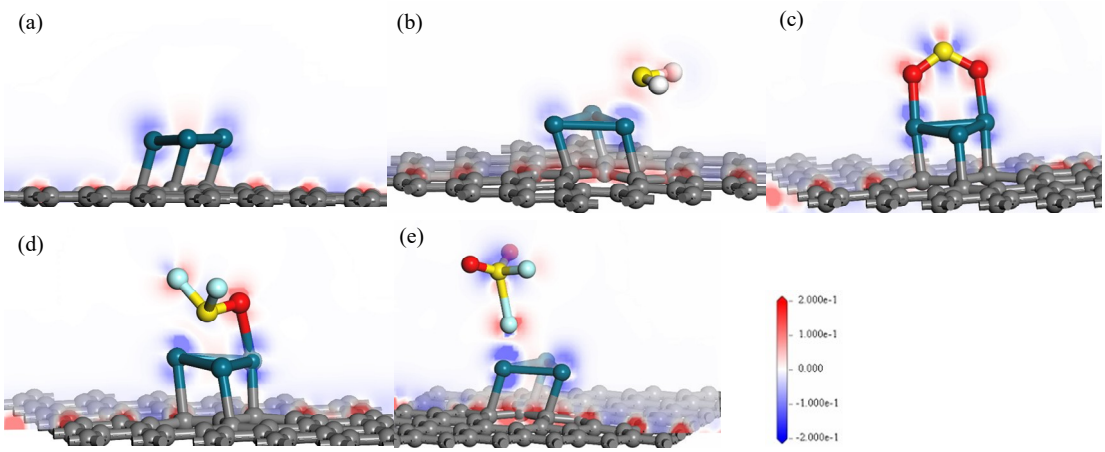

Figure 11. Deformation charge density (DCD) of pure Pd_3-graphene and the most stable adsorption structures. (**a**) Pure Pd_3-graphene; (**b**) H_2S; (**c**) SO_2; (**d**) SOF_2; (**e**) SO_2F_2.

According to the evident effect on the electronic structure of Pd_3-graphene after SF_6 product adsorption, the sensitivity and selectivity for application of chemical gas sensor must be further investigated. As a resistor-type gas sensor, the change in conductivity is an important factor in detecting SF_6 decomposition products. The conductivity (σ) of Pd_3-graphene gas sensor could be evaluated by the following formula [37]:

$$\sigma \propto e^{(-\frac{E_g}{2kT})},$$

where k, T and E_g represent the Boltzmann constant, temperature and HOMO–LUMO energy gap, respectively. Therefore, under a certain temperature condition, σ is an exponential function of the E_g and a smaller energy gap would determine a higher conductivity. We perform frontier molecular orbital theory to calculate the energy of HOMO (E_H) and LUMO (E_L) and obtain the specific E_g, which the difference between them.

Figure 12 intuitively presents the E_H, E_L and E_g of pristine Pd_3-graphene and the four most stable adsorption systems, where the black number represents the E_g. For pristine Pd_3-graphene, the E_g is 0.086 eV, signifying that the basic conductivity is relatively high, which probably results from the Pd_3 dopant. After gas adsorption, the E_g of different systems decreases without exception. While H_2S and SO_2 absorbing on the Pd_3-graphene surface in the most stable configuration, the E_g decreases by 13.95% and 9.30%, respectively, manifesting an increase in conductivity of the Pd_3-graphene sensor. For the SOF_2 adsorption system, the E_g of Pd_3-graphene decreases by 38.37%, which is the largest among the four adsorption systems, indicating that the electronic structure is more continuous, and the electronic transition is effortless. However, for the SO_2F_2 adsorption system, E_g reduces with the smallest degree, only 5.81%, which means the conductivity of the Pd_3-graphene sensor has a slight rise. In conclusion, the conductivity of Pd_3-graphene sensor increases after gas adsorption, which agrees with the analysis in the DOS part.

As for N_3&Ni doped 555–777 graphene reported in [36], N_3&Ni-graphene has a high sensitivity on absorbing H_2S and SO_2 gas while the E_g decreases from 0.426 eV to 0.052 eV and 0.138 eV, respectively. Hence, the sensitivity of N_3&Ni-graphene may be higher than Pd_3-graphene while absorbing H_2S and SO_2 gas. However, it is toilsome for N_3&Ni-graphene to distinguish SOF_2 molecule and SO_2F_2 due to their similar E_g. The problem can be solved by using Pd_3-graphene gas sensor for its obviously different E_g of various adsorption systems. As a result, Pd_3-graphene can be a better gas sensor material on detecting SF_6 decomposition product.

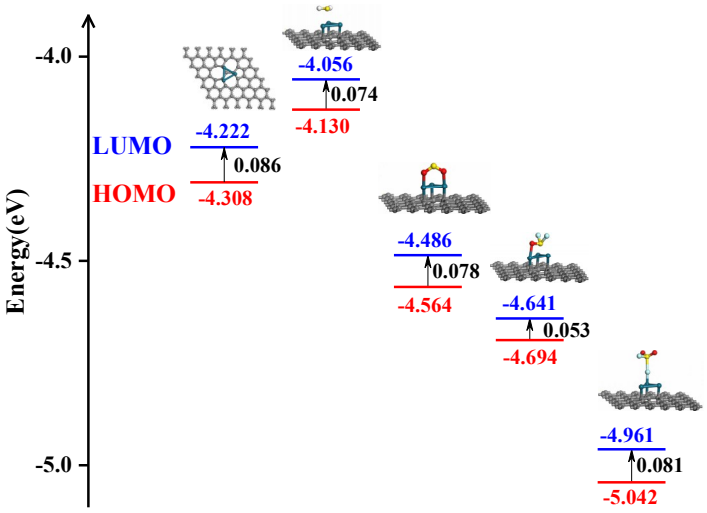

Figure 12. E_L, E_H and E_g of pristine Pd_3-graphene and various most stable adsorption systems. From the left to the right are pristine Pd_3-graphene, M1, M4, M7 and M8 systems, respectively.

4. Conclusions

In this work, we propose Pd_3-cluster-doped 555–777 graphene as a novel resistor-type gas sensor to detect SF_6 decomposition products (H_2S, SO_2, SOF_2 and SO_2F_2), and the calculation results are as follows:

(I) Adsorption energies of the most stable adsorption systems of H_2S, SO_2, SOF_2 and SO_2F_2 are −1.211, −1.591, −1.282 and −0.920 eV, respectively, demonstrating that the four gases could be absorbed on Pd_3-graphene surface by chemisorption. Charge transfer makes various atoms form ionic bonds during adsorption. In addition, the change of DOS and PDOS verifies high hybridizations of different atomic orbits.

(II) The conductivity of Pd_3-graphene would be improved without exception due to the decrease of E_g after gas adsorption. SOF_2 gas adsorption leads to the largest increase, whereas SO_2F_2 is the smallest. According to the reduced value of E_g, the sensitivity of the four gases follows the order SOF_2 > H_2S > SO_2 > SO_2F_2.

Thus, we confirm that Pd_3-graphene can absorb SF_6 decomposition products, and the Pd_3-graphene sensor can be employed to evaluate the insulation condition of GIS by detecting these decompositions.

Author Contributions: Conceptualization and methodology, J.L. and L.P.; software, formal analysis, data curation and writing—original draft preparation, J.L.; writing—review and editing, F.C., X.Y. and F.K. All authors have read and agreed to the published version of the manuscript.

Funding: This research received no external funding.

Acknowledgments: We gratefully acknowledge the financial support from the National Key Research and Development Program of China under Grant 2017YFB0902500 and the Science and Technology Project of SGCC through the Key Technology of Environment Friendly Gas-Insulated Transmission Line.

Conflicts of Interest: The authors declare no conflict of interest.

References

1. Knobloch, H. The Comparison of Arc-Extinguishing Capability of Sulfur Hexafluoride (SF_6) with Alternative Gases in High-Voltage Circuit-Breakers. In *Gaseous Dielectrics VIII*; Springer: Boston, MA, USA, 1998; pp. 565–571.
2. Chee-Hing, D.J.; Srivastava, K.D. Insulation Performance of Dielectric-Coated Electrodes in Sulphur Hexafluoride Gas. *IEEE Trans. Electr. Insul.* **1975**, *EI-10*, 119–124. [CrossRef]
3. Sauers, I. By-product formation in spark breakdown of SF_6/O_2 mixtures. *Plasma Chem. Plasma Process.* **1988**, *8*, 247–262. [CrossRef]

4. Casanovas, A.M.; Casanovas, J.; Lagarde, F.; Belarbi, A. Study of the decomposition of SF_6 under dc negative polarity corona discharges (point-to-plane geometry): Influence of the metal constituting the plane electrode. *J. Appl. Phys.* **1992**, *72*, 3344–3354. [CrossRef]
5. Zhang, X.; Gui, Y.; Dai, Z. Adsorption of gases from SF_6 decomposition on aluminum-doped SWCNTs: A density functional theory study. *Eur. Phys. J. D* **2015**, *69*, 185. [CrossRef]
6. Ju, T.; Fan, L.; Meng, Q.; Zhang, X.; Tao, J. Partial discharge recognition through an analysis of SF_6 decomposition products part 2: Feature extraction and decision tree-based pattern recognition. *IEEE Trans. Dielectr. Electr. Insul.* **2012**, *19*, 37–44.
7. Zhang, X.; Chen, Q.; Hu, W.; Zhang, J. A DFT study of SF_6 decomposed gas adsorption on an anatase (101) surface. *Appl. Surf. Sci.* **2013**, *286*, 47–53. [CrossRef]
8. Ju, T.; Zeng, F.; Pan, J.; Zhang, X.; Qiang, Y.; He, J.; Hou, X. Correlation analysis between formation process of SF_6 decomposed components and partial discharge qualities. *IEEE Trans. Dielectr. Electr. Insul.* **2013**, *20*, 864–875.
9. Fridman, A.; Chirokov, A.; Gutsol, A. Non-Thermal Atmospheric Pressure Discharges. *J. Phys. D Appl. Phys.* **2005**, *38*, R1. [CrossRef]
10. Kóréh, O.; Rikker, T.; Molnár, G.; Mahara, B.M.; Torkos, K.; Borossay, J. Study of decomposition of sulphur hexafluoride by gas chromatography/mass spectrometry. *Rapid Commun. Mass Spectrom.* **1997**, *11*, 1643–1648. [CrossRef]
11. Zhang, X.X.; Wang, Z.; Hu, Y.G.; Ren, J.B. Recognition of SF_6 decomposition components by two-dimensional infrared spectroscopy. *Gaodianya Jishu/High Volt. Eng.* **2010**, *36*, 1475–1479.
12. Yuan, W.; Shi, G. Graphene-based gas sensors. *J. Mater. Chem. A* **2013**, *1*, 10078–10091. [CrossRef]
13. Liu, J. Adsorption of DNA onto gold nanoparticles and graphene oxide: Surface science and applications. *Phys. Chem. Chem. Phys.* **2012**, *14*, 10485–10496. [CrossRef]
14. Wei, W.; Nong, J.; Zhang, G.; Tang, L.; Zhu, Y. Graphene-Based Long-Period Fiber Grating Surface Plasmon Resonance Sensor for High-Sensitivity Gas Sensing. *Sensors* **2016**, *17*, 2. [CrossRef] [PubMed]
15. Singh, G.; Choudhary, A.; Haranath, D.; Joshi, A.G.; Singh, N.; Singh, S.; Pasricha, R. ZnO decorated luminescent graphene as a potential gas sensor at room temperature. *Carbon* **2012**, *50*, 385–394. [CrossRef]
16. Cen, C.; Zhang, Y.; Chen, X.; Yang, H.; Wu, P. A dual-band metamaterial absorber for graphene surface plasmon resonance at terahertz frequency. *Phys. E Low-Dimens. Syst. Nanostruct.* **2020**, *117*, 113840. [CrossRef]
17. Wu, P.; Chen, Z.; Xu, D.; Zhang, C.; Jian, R. A Narrow Dual-Band Monolayer Unpatterned Graphene-Based Perfect Absorber with Critical Coupling in the Near Infrared. *Micromachines* **2020**, *11*, 58. [CrossRef]
18. Banhart, F.; Kotakoski, J.; Krasheninnikov, A.V. Structural Defects in Graphene. *ACS Nano* **2011**, *5*, 26–41. [CrossRef]
19. Liu, P.; Fu, C.; Li, Y.; Wei, H. Theoretical screening of single atom anchored on defective graphene for electrocatalytic N_2 reduction reactions: A DFT study. *Phys. Chem. Chem. Phys.* **2020**, *22*, 9322–9329. [CrossRef]
20. Arokiyanathan, A.L.; Panjulingam, N.; Lakshmipathi, S. Chemical Properties of Lithium Cluster (Lix, x = 2–8) on Stone–Wales Defect Graphene Sheet: A DFT Study. *J. Phys. Chem. C* **2020**, *124*, 7229–7237. [CrossRef]
21. Ma, S.; Chen, J.; Wang, L.; Jiao, Z. First-principles insight into hydrogen adsorption over Co-4 anchored on defective graphene. *Appl. Surf. Sci.* **2020**, *504*, 144413. [CrossRef]
22. Olsson, E.; Hussain, T.; Karton, A.; Cai, Q. The adsorption and migration behavior of divalent metals (Mg, Ca, and Zn) on pristine and defective graphene. *Carbon* **2020**, *163*, 276–287. [CrossRef]
23. Guan, Z.Y.; Ni, S.; Hu, S. First-Principles Study of 3d Transition-Metal-Atom Adsorption onto Graphene Embedded with the Extended Line Defect. *ACS Chem. Biol.* **2020**, *5*, 5900–5910. [CrossRef]
24. Zhang, J.; Deng, Y.; Cai, X.; Chen, Y.; Peng, M.; Jia, Z.; Jiang, Z.; Ren, P.; Yao, S.; Xie, J. Tin Assisted Fully Exposed Platinum Clusters Stabilized on Defect-Rich Graphene for Dehydrogenation Reaction. *ACS Catal.* **2019**, *9*, 5998–6005. [CrossRef]
25. Olsson, E.; Chai, G.; Dove, M.; Cai, Q. Adsorption and migration of alkali metals (Li, Na, and K) on pristine and defective graphene surfaces. *Nanoscale* **2019**, *11*, 5274–5284. [CrossRef] [PubMed]
26. Gui, Y.; Peng, X.; Liu, K.; Ding, Z. Adsorption of C_2H_2, CH_4 and CO on Mn-doped graphene: Atomic, electronic, and gas-sensing properties. *Phys. E Low-Dimens. Syst. Nanostruct.* **2020**, *119*, 113959. [CrossRef]

27. Gao, X.; Zhou, Q.; Wang, J.; Xu, L.; Zeng, W. Adsorption of SO_2 molecule on Ni-doped and Pd-doped graphene based on first-principle study. *Appl. Surf. Sci.* **2020**, *517*, 146180. [CrossRef]
28. Zhang, X.; Cui, H.; Gui, Y. Synthesis of Graphene-Based Sensors and Application on Detecting SF_6 Decomposing Products: A Review. *Sensors* **2017**, *17*, 363. [CrossRef]
29. Bae, G.; Jeon, I.S.; Jang, M.; Song, W.; Myung, S.; Lim, J.; Lee, S.S.; Jung, H.-K.; Park, C.-Y.; An, K.-S. Complementary Dual-Channel Gas Sensor Devices Based on a Role-Allocated ZnO/Graphene Hybrid Heterostructure. *ACS Appl. Mater. Interfaces* **2019**, *11*, 16830–16837. [CrossRef]
30. Liu, D.; Gui, Y.; Ji, C.; Tang, C.; Zhou, Q.; Li, J.; Zhang, X. Adsorption of SF_6 decomposition components over Pd (111): A density functional theory study. *Appl. Surf. Sci.* **2019**, *465*, 172–179. [CrossRef]
31. Delley, B.J. From Molecules to Solids with the $DMol^3$ Approach. *J. Chem. Phys.* **2000**, *113*, 7756–7764. [CrossRef]
32. White, J.A.; Bird, D.M. Implementation of gradient-corrected exchange-correlation potentials in Car-Parrinello total-energy calculations. *Phys. Rev. B Condens. Matter* **1994**, *50*, 4954–4957. [CrossRef] [PubMed]
33. Perdew, J.P.; Burke, K.; Ernzerhof, M. Generalized gradient approximation made simple. *Phys. Rev. Lett.* **1996**, *77*, 3865–3868. [CrossRef]
34. Monkhorstand, H.J.; Pack, J.D. Special points for Brillouin-zoneintegrations. *Phys. Rev. B* **1977**, *16*, 5188–5192.
35. Delley, B. An all-electron numerical method for solving the local density functional for polyatomic molecules. *J. Chem. Phys.* **1990**, *92*, 508. [CrossRef]
36. Li, J.; Pang, L.; He, K.; Zhang, L. Theoretical Study of The Gas Sensing Mechanism of N_3&Ni Doped Double Vacancies Defect Graphene upon SF_6 Decompositions. *IEEE Access* **2019**, *7*, 145567–145573.
37. Li, S.S. *Semiconductor Physical Electronics*; Springer Science & Business Media: Berlin/Heidelberg, Germany, 2006.